Higgs-flavon mixing and LHC phenomenology in a simplified model of broken flavor symmetry

Edmond L. Berger, Steven B. Giddings, Haichen Wang, and Hao Zhang

Higgs-flavon mixing and LHC phenomenology
in a simplified model of broken flavor symmetry

Edmond L. Berger,[1, *] Steven B. Giddings,[2, †] Haichen Wang,[3, ‡] and Hao Zhang[2, 4, §]

[1]*High Energy Physics Division, Argonne National Laboratory, Argonne, IL 60439, USA*
[2]*Department of Physics, University of California, Santa Barbara, CA 93106, USA*
[3]*Lawrence Berkeley National Laboratory, Berkeley, CA 94720, USA*
[4]*Center for High Energy Physics, Peking University, Beijing 100871, China*

The LHC phenomenology of a low-scale gauged flavor symmetry model with inverted hierarchy is studied, through introduction of a simplified model of broken flavor symmetry. A new scalar (a flavon) and a new neutral top-philic massive gauge boson emerge with mass in the TeV range along with a new heavy fermion associated with the standard model top quark. After checking constraints from electroweak precision observables, we investigate the influence of the model on Higgs boson physics, notably on its production cross section and decay branching fractions. Limits on the flavon φ from heavy Higgs boson searches at the LHC at 7 and 8 TeV are presented. The branching fractions of the flavon are computed as a function of the flavon mass and the Higgs-flavon mixing angle. We also explore possible discovery of the flavon at 14 TeV, particularly via the $\varphi \to Z^0 Z^0$ decay channel in the $2\ell 2\ell'$ final state, and through standard model Higgs boson pair production $\varphi \to hh$ in the $b\bar{b}\gamma\gamma$ final state. We conclude that the flavon mass range up to 500 GeV could probed down to quite small values of the Higgs-flavon mixing angle with 100 fb^{-1} of integrated luminosity at 14 TeV.

I. INTRODUCTION

The standard model (SM) of particle physics describes physics at the electroweak symmetry breaking (EWSB) scale of the visible sector remarkably well. With the discovery of a Higgs boson behaving much like that of the SM at the Large Hadron Collider (LHC) [1, 2], all of the expected SM particles have been detected. Attention has turned to precise determination of the properties of the Higgs boson, notably its decay branching fractions, and to the search for possible new physics beyond the SM. Given current precision, the branching fractions allow some, if limited, deviations from SM predictions.

The SM poses several puzzles. These include the origin of the fermion mass hierarchy and the flavor structure parametrized in the well-known CKM matrix [3, 4]. The dynamics of flavor mixing is well described within a framework of three generations of quarks. The fact that no significant deviations from SM predictions have appeared in any flavor-related physics processes indicates that that any TeV scale new physics (NP) does not introduce any important new source of flavor change or CP violation beyond the SM. This hints at flavor symmetry (horizontal symmetry) in a NP model. The idea that the NP interactions are invariant under a flavor symmetry group is known as minimal flavor violation (MFV) [5].

In the MFV scenario, the SM flavor symmetry is broken explicitly by the non-vanishing SM Yukawa coupling constants. This symmetry could nevertheless be a true symmetry of nature at some high energy scale but broken by non-zero vacuum expectation values (vev's) of scalar fields which are usually called flavons. In such a case, the SM Yukawa coupling constants are related to the ratio between the vev's of flavons and some cutoff scale.

If the full non-abelian flavor symmetry of the fermion kinetic terms and gauge couplings is a global symmetry broken by flavons, this yields Goldstone bosons subject to stringent constraints. This problem can be avoided if the non-abelian flavor symmetry is gauged, giving mass to the Goldstone modes.[1] Anomaly cancellation in such a theory requires introduction of exotic fermions[10–15] to cancel gauge anomalies. These mix with the SM fermions. The SM fermion masses are the smaller eigenvalues of the mass matrix and are proportional to the inverse of the flavon vev's, corresponding to an inverted hierarchy. The masses of all NP particles, such as the extra fermions, flavons, and flavor gauge bosons, are controlled by the flavon vev's and therefore are approximately proportional to the inverse of the SM Yukawa constants. Constraints from low energy precision observables and flavor physics are carefully considered in [13, 16].

The lightest new particles in such a flavor symmetry model with inverted hierarchy are the exotic fermions, the flavon which couples to the third generation of SM fermions, and a massive top-philic gauge boson. Their masses could be at the TeV scale, and it should be possible to search for them at the LHC. The LHC phenomenol-

---

* berger@anl.gov
† giddings@physics.ucsb.edu
‡ haichenwang@lbl.gov
§ zhanghao@physics.ucsb.edu

---

[1] Other scenarios include abelian flavor symmetries [6, 7], discrete flavor symmetries [8], and the little Higgs mechanism [9]; these are not considered in this work.

ogy of the flavon, the top-philic gauge boson and the heavy fermion partner of the top-quark might be interestingly rich.

In this paper we do not focus on details of flavor physics *per se*. Rather, we address the implications of flavons and the heavy fermion partner of the top-quark for Higgs boson physics, and the LHC phenomenology of a simplified flavor symmetry model with inverted hierarchy. We begin in Sec. II with an explanation of the motivation and origin for the inverted hierarchy in a flavor symmetry model. The simplified Lagrangian and the mass eigenstates are shown in this section also. In Sec. III, we briefly review the constraints from electroweak precision observables (EWPO) and flavor violation experiments. We study the effects of the flavor symmetry model on the production and decay properties of the SM Higgs boson in Sec. IV. The inclusive Higgs boson production cross section is suppressed relative to the SM by a factor $c_H^2 = \cos^2 \theta_H$, where θ_H is the mixing angle of the scalar flavon and the Higgs boson. This suppression is allowed by the LHC data at 7 and 8 TeV, within limits. We show that most of the Higgs boson couplings to SM particles are just rescaled by a factor c_H, including the loop induced hgg and $h\gamma\gamma$ vertices in the heavy fermion limit. The $hZ^0\gamma$ vertex deviates from the simple c_H rescaling, but the deviation is small. The Higgs boson decay branching ratios are nearly unchanged relative to the SM since every sizable partial width is changed by an overall factor c_H^2. In Sec. V, we investigate limits on the flavon from LHC data at 7 and 8 TeV and possible signals of the flavon at 14 TeV. Flavon searches at the LHC can focus on the SM Higgs-like decay channels (Z^0Z^0, W^+W^-) and on the Higgs boson pair decay channel $\varphi \to hh$. We compute and display the decay branching fractions of the flavon as a function of the flavon mass and mixing angle θ_H. Only the W^+W^-, Z^0Z^0, hh and $t\bar{t}$ channels are significant in flavon decay. We examine bounds on the parameter space of flavons from heavy Higgs boson searches at 7 and 8 TeV. Because the flavon can be produced singly, if it decays into the hh final state with an appreciable decay branching ratio, the Higgs pair cross section will be enhanced significantly by this resonance effect. We perform a detailed simulation of the signal and backgrounds for the $\varphi \to hh \to b\bar{b}\gamma\gamma$ channel at 14 TeV for an assumed integrated luminosity of 100fb^{-1}, deriving both 2 standard deviation exclusion limits and 5 standard deviation observation bounds as a function of flavon mass. In some regions of parameter space the search for a hh signal will give a stronger constraint on the NP model than the Z^0Z^0 channel. Our conclusions are summarized in Sec. VI.

II. FROM GAUGED FLAVOR SYMMETRY TO A SIMPLIFIED MODEL OF BROKEN FLAVOR SYMMETRY

The flavor symmetry of the quark kinetic terms and gauge couplings is

$$G_f = U(3)_{Q_L} \otimes U(3)_{U_R} \otimes U(3)_{D_R} \ , \qquad (1)$$

If this symmetry is gauged with only SM fermions present, the theory is anomalous. A "minimal" model of new fermions that cancel the anomalies was described in [13]. This model has exotic fermion partners of the SM quarks, flavor gauge bosons, and two scalar flavon fields Y_u and Y_d for the up-like and down-like quarks. $U(1)_{Q_L}$ remains anomalous, but the rest of the flavor symmetry (1) is taken to be gauged. The most general renormalizable interaction Lagrangian between the flavon fields and the SM and exotic fermions takes the form

$$
\begin{aligned}
\mathcal{L}_{\text{UV}} = \ &\mathcal{L}_{\text{kinetic + gauge}} \\
&-(-\lambda_u \bar{Q}_L \tilde{H} \Psi_{uR} + \lambda'_u \bar{\Psi}_u Y_u \Psi_{uR} + M_u \bar{\Psi}_u U_R \\
&\ -\lambda_d \bar{Q}_L H \Psi_{dR} + \lambda'_d \bar{\Psi}_d Y_d \Psi_{dR} + M_d \bar{\Psi}_d D_R + \text{h.c.}) \\
&-V(Y_u, Y_d, H) \ . \qquad (2)
\end{aligned}
$$

Here Q_L, U_R, D_R are the SM quark fields, Ψ_u, Ψ_{uR}, Ψ_d, and Ψ_{dR} are the partner fermion fields, H is the SM Higgs doublet field, and $\tilde{H}_i \equiv \varepsilon_{ij} H_j$ where ε_{ij} is the antisymmetric tensor with $\varepsilon_{12} = 1$. λ and λ' are dimensionless parameters, M is a parameter with the dimensions of mass, and V is the scalar potential. The representations under the gauge groups to which these these fields belong is shown in TABLE I. One can verify that both the SM gauge symmetry and the flavor gauge symmetry are anomaly free with the contributions from the exotic fermion fields. If flavor symmetry breaks via flavon vevs with $\langle Y \rangle \gg M$, the masses of the SM fermions are inversely proportional to the vev of the corresponding flavon field component, resulting in the asserted inverted hierarchy.

The large hierarchy between the masses of the SM quarks thus corresponds to a large hierarchy between the vevs of the flavons which suggests that the flavor symmetry could be broken sequentially [17]. Guided by this realization, we assume that the breaking of the Lagrangian in Eq (2) occurs in a sequence of steps. From the effective field theory point of view, one successively integrates out heavy degrees of freedom.

If we integrate out the heavy degrees of freedom associated with the first and second generations, we are left with a simplified flavor symmetry model with a manageable number of BSM degrees of freedom (a flavon, an exotic fermion, and a massive vector boson) associated with the top-quark and bottom-quark sectors. However, because the vev of the flavon associated with the bottom-quark is nearly two orders of magnitude larger than the vev of the flavon associated with the top-quark, this suggests finally integrating out the flavon associated with

TABLE I. The representation of the fields in Eq (2) under the SM gauge group and the flavor symmetry group.

	$SU(3)_{Q_L}$	$SU(3)_{U_R}$	$SU(3)_{D_R}$	$SU(3)_c$	$SU(2)_L$	$U(1)_Y$
Q_L	3	1	1	3	2	1/6
U_R	1	3	1	3	1	2/3
D_R	1	1	3	3	1	-1/3
Ψ_u	1	3	1	3	1	2/3
Ψ_d	1	1	3	3	1	-1/3
Ψ_{uR}	3	1	1	3	1	2/3
Ψ_{dR}	3	1	1	3	1	-1/3
Y_u	$\bar{3}$	3	1	1	1	0
Y_d	$\bar{3}$	1	3	1	1	0
H	1	1	1	1	2	1/2

the bottom-quark. Thus, at the TeV scale, we have the effective Lagrangian

$$\mathcal{L}_{\text{topflavor}} = \lambda \bar{Q}_L \tilde{H} \Psi_{tR} - \lambda' \bar{\Psi}_t \Phi \Psi_{tR} - M \bar{\Psi}_t t_R + \text{h.c.}, \quad (3)$$

where Φ is a complex flavon associated with the top-quark. There is also a residual $U(1)$ gauged flavor symmetry under which only the Φ, Ψ_t and t_R fields carry (the same) charge. Chiral phase rotations of the fermions allow us to take, without loss of generality, $\lambda, \lambda', M > 0$. We can consider the Lagrangian (3) separately from our discussion of the higher-scale flavor structure, as a simplified model extending the top and Higgs sectors. The usual SM Yukawa interactions for the remaining fermions are added to this Lagrangian.[2]

After EWSB and FSB,

$$H = \begin{pmatrix} 0 \\ \frac{v+\tilde{h}}{\sqrt{2}} \end{pmatrix}, \quad (4)$$

$$\Phi = \frac{\tilde{\varphi} + v_\varphi}{\sqrt{2}}, \quad (5)$$

in the unitary gauge, where $v = 246$ GeV is the vev of the Higgs field, $\tilde{h}$ is the physical degree of freedom of the SM Higgs doublet field, and $\tilde{\varphi}$ is the physical degree of freedom of the top flavon. The mass eigenstates are linear combinations of $\tilde{h}$ and $\tilde{\varphi}$ which will be given below.

The mass matrix of the fermions is

$$\mathcal{L}_M = -\begin{pmatrix} \bar{t}_L & \bar{\Psi}_t \end{pmatrix} \begin{pmatrix} 0 & -\lambda v/\sqrt{2} \\ M & \lambda' v_\varphi/\sqrt{2} \end{pmatrix} \begin{pmatrix} t_R \\ \Psi_{tR} \end{pmatrix}. \quad (6)$$

It can be diagonalized by separate left and right rota-

---

[2] There are other models with similar Lagrangians, although arising from different motivations. For example, see [18, 19].

tions. This results in mass eigenvalues given by

$$m_t^2 = \frac{1}{4}\left[-\sqrt{\left(2M^2 + \lambda^2 v^2 + \lambda'^2 v_\varphi^2\right)^2 - 8\lambda^2 M^2 v^2} + 2M^2 + \lambda^2 v^2 + \lambda'^2 v_\varphi^2\right],$$

$$m_T^2 = \frac{1}{4}\left[\sqrt{\left(2M^2 + \lambda^2 v^2 + \lambda'^2 v_\varphi^2\right)^2 - 8\lambda^2 M^2 v^2} + 2M^2 + \lambda^2 v^2 + \lambda'^2 v_\varphi^2\right], \quad (7)$$

which are positive and real for real λ, λ', M. Here m_t should be the running mass of the top quark which is 163 GeV [20]. One can find $\lambda' v_\varphi$ in terms of the other parameters, if m_t is fixed to be the mass of the SM top quark. Reality of $\lambda' v_\varphi$ requires

$$\left(M^2 - m_t^2\right)\left(\lambda^2 v^2 - 2m_t^2\right) > 0. \quad (8)$$

The case $m_t > M$ and $\lambda v < \sqrt{2} m_t$ would correspond to the SM top quark being the heavier fermion; we do not treat this scenario because a light colored fermion T which also couples to the electroweak gauge boson and the Higgs boson would be highly constrained by current data. Thus, T will denote the heavy partner of the top quark.

When $M > m_t$ and $\lambda v > \sqrt{2} m_t$, the other mass eigenvalue is

$$m_T = \frac{Mv\lambda}{\sqrt{2} m_t}. \quad (9)$$

The right and left components of the two fermion mass eigenstates, the SM top quark t and a heavy fermion T, are

$$\begin{pmatrix} t_R \\ \Psi_{tR} \end{pmatrix} = P_R \begin{pmatrix} \cos\theta_R & \sin\theta_R \\ -\sin\theta_R & \cos\theta_R \end{pmatrix} \begin{pmatrix} t \\ T \end{pmatrix}, \quad (10)$$

$$\begin{pmatrix} t_L \\ \Psi_t \end{pmatrix} = P_L \begin{pmatrix} \cos\theta_L & \sin\theta_L \\ -\sin\theta_L & \cos\theta_L \end{pmatrix} \begin{pmatrix} t \\ T \end{pmatrix}. \quad (11)$$

It is easy to derive

$$s_L \equiv \sin\theta_L = -\frac{m_t\sqrt{\lambda^2 v^2 - 2m_t^2}}{\sqrt{M^2 v^2 \lambda^2 - 2m_t^4}}, \quad (12)$$

$$c_L \equiv \cos\theta_L = \frac{\lambda v\sqrt{M^2 - m_t^2}}{\sqrt{M^2 v^2 \lambda^2 - 2m_t^4}}, \quad (13)$$

$$s_R \equiv \sin\theta_R = \frac{\sqrt{2} m_t\sqrt{M^2 - m_t^2}}{\sqrt{M^2 v^2 \lambda^2 - 2m_t^4}}, \quad (14)$$

$$c_R \equiv \cos\theta_R = \frac{M\sqrt{\lambda^2 v^2 - 2m_t^2}}{\sqrt{M^2 v^2 \lambda^2 - 2m_t^4}}. \quad (15)$$

The Yukawa interactions are therefore

$$\mathcal{L}_Y = \frac{\lambda \tilde{h}}{\sqrt{2}} \Big[-\bar{t}t c_L s_R + \bar{t}\left(-s_L s_R P_L + c_L c_R P_R\right)T$$
$$+ \bar{T}\left(c_L c_R P_L - s_L s_R P_R\right)t + \bar{T}T s_L c_R \Big]$$
$$- \frac{\lambda' \tilde{\varphi}}{\sqrt{2}} \Big[\bar{t}t s_L s_R - \bar{t}\left(c_L s_R P_L + s_L c_R P_R\right)T$$
$$- \bar{T}\left(s_L c_R P_L + c_L s_R P_R\right)t + \bar{T}T c_L c_R \Big], \quad (16)$$

while the gauge interactions are

$$\mathcal{L}_K = \frac{2e s_W}{3 c_W} \bar{T}\gamma^\mu \left[\left(1 - \frac{3 s_L^2}{4 s_W^2}\right)P_L + P_R \right] T Z_\mu$$
$$+ \frac{2e s_W}{3 c_W} \bar{t}\gamma^\mu \left[\left(1 - \frac{3 c_L^2}{4 s_W^2}\right)P_L + P_R \right] t Z_\mu$$
$$- \frac{e s_L c_L}{2 s_W c_W}\left(\bar{t}\gamma^\mu P_L T + \bar{T}\gamma^\mu P_L t\right)Z^\mu$$
$$- \frac{e c_L}{\sqrt{2} s_W}\bar{t}\gamma^\mu P_L b W^+_\mu - \frac{e c_L}{\sqrt{2} s_W}\bar{b}\gamma^\mu P_L t W^-_\mu$$
$$- \frac{e s_L}{\sqrt{2} s_W}\bar{T}\gamma^\mu P_L b W^+_\mu - \frac{e s_L}{\sqrt{2} s_W}\bar{b}\gamma^\mu P_L T W^-_\mu$$
$$- \frac{2e}{3}\bar{t}\gamma^\mu t A_\mu - \frac{2e}{3}\bar{T}\gamma^\mu T A_\mu, \quad (17)$$

where s_W (c_W) is the sine (cosine) of the weak angle.

In the scalar potential, the trilinear interaction between Φ and H is forbidden by the $SU(2)_L$ and flavor symmetries. However, the interaction

$$(\Phi^*\Phi)(H^\dagger H) \quad (18)$$

is still allowed. This term can be generated through a combined top-quark and heavy fermion T loop in the one-loop effective potential even it is forbidden artificially at tree-level (FIG. 1). The general renormalizable La-
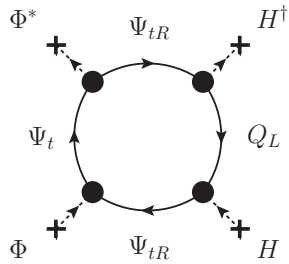

FIG. 1. Contribution to the one-loop effective potential from Eq (3). Each black dot means an insertion of the vertex and a zero-momentum external scalar.

grangian of the scalar fields of the complex gauge singlet extension of the SM can be written as

$$\mathcal{L} = \left(D_\mu H\right)^\dagger \left(D^\mu H\right) + \left(D_\mu \Phi\right)^* \left(D^\mu \Phi\right) - V\left(H, \Phi\right) \quad (19)$$

with scalar potential

$$V\left(H, \Phi\right) = \frac{\lambda_H}{2}\left(H^\dagger H\right)^2 + \frac{\lambda_\Phi}{2}\left(\Phi^*\Phi\right)^2 - \frac{1}{2}m_H^2\left(H^\dagger H\right)$$
$$- \frac{1}{2}m_\Phi^2(\Phi^*\Phi) + \xi(\Phi^*\Phi)\left(H^\dagger H\right) ; \quad (20)$$

the parameters λ_H and λ_Φ describe the self-interactions of the Higgs field and the flavon field. The gauge covariant derivative of the SM doublet Higgs field is the same as the one in the SM. The gauge covariant derivative of the flavon is

$$D_\mu \Phi = \partial_\mu \Phi - i g_T Z_{T\mu}\Phi, \quad (21)$$

where g_T is the gauge coupling constant of the residual $U(1)$ flavor gauge symmetry, and $Z_{T\mu}$ is the gauge field of the residual $U(1)$ flavor gauge symmetry.

The vev's of neutral components are found to be

$$v = \sqrt{\frac{\lambda_\Phi m_H^2 - \xi m_\Phi^2}{\lambda_H \lambda_\Phi - \xi^2}}, \quad (22)$$

$$v_\varphi = \sqrt{\frac{\lambda_H m_\Phi^2 - \xi m_H^2}{\lambda_H \lambda_\Phi - \xi^2}}. \quad (23)$$

Avoidance of a flat direction of the vacuum requires

$$\lambda_H \lambda_\Phi - \xi^2 > 0. \quad (24)$$

The vev of the $SU(2)_L$ doublet field is determined by the weak interaction coupling constant and the masses of the SM massive gauge bosons. Therefore there is a constraint

$$\sqrt{\frac{\lambda_\Phi m_H^2 - \xi m_\Phi^2}{\lambda_H \lambda_\Phi - \xi^2}} = 246\text{GeV}. \quad (25)$$

The physical degree of freedom which is dominated by $\tilde{h}$ should be the SM-like Higgs boson h. Its mass should be $m_h = 125.4$ GeV [21, 22]. Assuming the other scalar field mass eigenstate has mass m_φ, we can solve for the parameters m_H and ξ, and present the results in terms of $m_h, v, m_\varphi, \lambda_H$ and λ_Φ, where the first two parameters are determined by current experiments. We can also determine λ' using these parameters as

$$\lambda' = \frac{1}{m_t}\sqrt{\frac{\lambda_\Phi\left(M^2 - m_t^2\right)\left(\lambda^2 v^2 - 2m_t^2\right)}{m_\varphi^2 + m_h^2 - \lambda_H v^2}}. \quad (26)$$

We define the mass eigenstates (h, φ) of the scalar fields by

$$\begin{pmatrix} \tilde{h} \\ \tilde{\varphi} \end{pmatrix} = \begin{pmatrix} \cos\theta_H & \sin\theta_H \\ -\sin\theta_H & \cos\theta_H \end{pmatrix}\begin{pmatrix} h \\ \varphi \end{pmatrix}, \quad (27)$$

where the rotation angle θ_H is given by

$$\sin\theta_H = \sqrt{\frac{\lambda_H v^2 - m_h^2}{m_\varphi^2 - m_h^2}}, \quad (28)$$

$$\cos\theta_H = \sqrt{\frac{m_\varphi^2 - \lambda_H v^2}{m_\varphi^2 - m_h^2}}. \quad (29)$$

The deviation of the Higgs field self-interaction strength λ_H from its value $\lambda_H^{SM} = m_h^2/v^2$ in the SM can be written as

$$\lambda_H \equiv \lambda_H^{SM} + \frac{m_\varphi^2 - m_h^2}{v^2}\sin^2\theta_H. \qquad (30)$$

The additional massive gauge boson $Z_{T\mu}$, whose mass is $m_{Z_T} = g_T\sqrt{\left(m_\varphi^2 c_H^2 + m_h^2 s_H^2\right)/\lambda_\Phi}$, couples at tree-level only to the SM top-quark, the heavy fermion, the flavon, and the Higgs boson through

$$\begin{aligned}
\mathcal{L} = {}& g_T Z_{T\mu}\big[\bar{t}\gamma^\mu\left(s_L^2 P_L + c_R^2 P_R\right)t + \bar{T}\gamma^\mu\left(c_L^2 P_L + s_R^2 P_R\right)T \\
& - \bar{t}\gamma^\mu\left(s_L c_L P_L - s_R c_R P_R\right)T - \bar{T}\gamma^\mu\left(s_L c_L P_L - s_R c_R P_R\right)t\big] \\
& + g_T m_{Z_T} c_H \varphi Z_T^\mu Z_{T\mu} - g_T m_{Z_T} s_H h Z_{T\mu} Z_T^\mu \\
& + \frac{1}{2}g_T^2 c_H^2 \varphi^2 Z_{T\mu} Z_T^\mu + \frac{1}{2}g_T^2 s_H^2 h^2 Z_{T\mu} Z_T^\mu \\
& - g_T^2 s_H c_H h \varphi Z_{T\mu} Z_T^\mu.
\end{aligned} \qquad (31)$$

Searching for such a top-philic gauge boson is a challenging task at colliders when it does not mix with the SM Z^0 at tree-level [23–27].

In summary, this section has presented a simplified model of spontaneous flavor symmetry breaking, which arises from the the gauged flavor symmetry model with inverted hierarchy in which only degrees of freedom related to the third generation are considered. There is a heavy fermion T which mixes with the SM top-quark, a heavy scalar flavon φ which mixes with the SM-like Higgs boson, and a heavy top-philic vector boson $Z_{T\mu}$. The basic couplings that we will need have been presented in this section.

III. CONSTRAINTS FROM THE ELECTROWEAK PRECISION OBSERVABLES

The interactions between the fermions and the SM gauge bosons are different in the low-scale gauged flavor symmetry model from the SM interactions. The new scalar also couples to the SM gauge bosons such that the strength of these interactions should be constrained by SM electroweak precision observables [28]. The modification of the charged current will also change the prediction of $b \to s\gamma$. Constraints from the EWPO and flavor physics were considered in the original paper [13]. In this work, we rexamine the EWPO constraints and include the contribution from the flavon φ in our calculation.

Because the new physics effects occur above the Z-pole, their influence on the SM EWPO can be described with the well known oblique parameters S, T, U [29]. When the SM reference values of m_t and m_h are chosen to be

$$m_{h,\mathrm{ref}} = 126\mathrm{GeV}, \quad m_{t,\mathrm{ref}} = 173\mathrm{GeV}, \qquad (32)$$
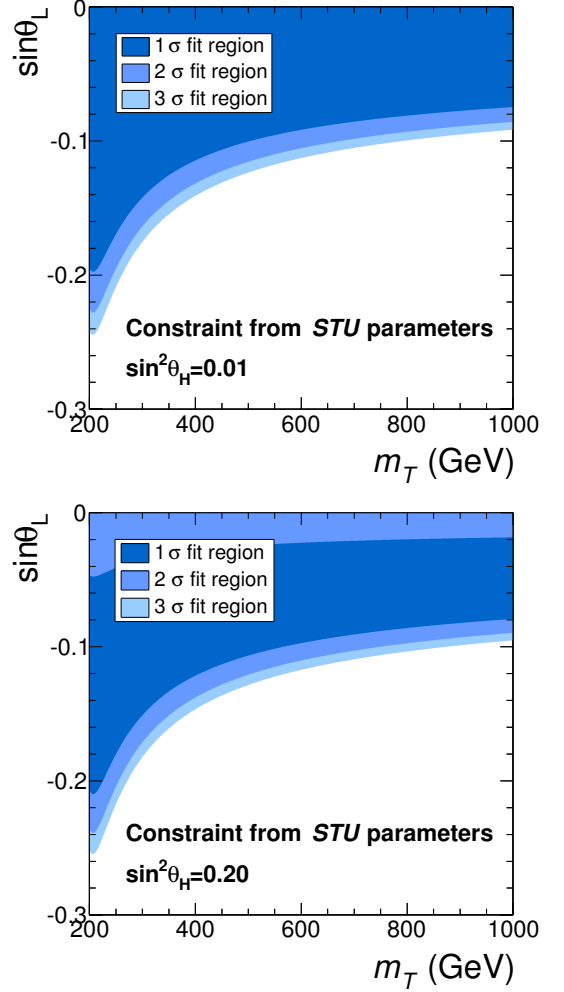

FIG. 2. The constraint on the mass of the heavy fermion m_T and the mixing angle of the left handed fermions s_L from the electroweak oblique parameters. The flavon mass m_φ is chosen to be 300 GeV. In the upper panel, the scalar mixing angle is $s_H^2 = 0.01$. In the lower panel, $s_H^2 = 0.20$.

the best fit values of the oblique parameters are [30]

$$\begin{aligned}
S &= 0.03 \pm 0.10, \\
T &= 0.05 \pm 0.12, \\
U &= 0.03 \pm 0.10,
\end{aligned} \qquad (33)$$

while the correlation coefficients matrix is [30]

$$\begin{pmatrix}
1 & 0.89 & -0.54 \\
0.89 & 1 & -0.83 \\
-0.54 & -0.83 & 1
\end{pmatrix}. \qquad (34)$$

The contribution from the exotic real scalar boson φ to the oblique parameters [31] is suppressed by the mixing angle θ_H. The contribution from the third generation is given in [13]. Using a χ^2 check, we show the one standard deviation (1σ), 2σ and 3σ fit regions in FIG. 2. A detailed analysis of $\Delta F = 2$ flavor physics observables and

of $B \to X_s\gamma$ in this model is presented in Ref. [16]. After inclusion of the contributions from the gauge bosons of the flavor group, this model could resolve the $\varepsilon_K - S_{\psi K_S}$ tension but result in a more serious tension from $\Delta M_{B_{d,s}}$ and $R_{BR/\Delta M}$ than in the SM. Contributions from the flavons are not included. Interested readers can find the constraints in Ref. [16]. The tension from flavor physics comes from the off-diagonal flavor gauge bosons (which are heavy and integrated out in our simplified model). They introduce additional tree-level flavor-changing neutral current (FCNC) processes. However, we do not discuss them numerically since they do not constrain the top-flavon sector.

IV. HIGGS BOSON PHYSICS

In this section, we investigate Higgs boson physics in the simplified flavor symmetry model under consideration. The interactions between the SM-like Higgs boson and other SM particles are different from those in the pure SM. The differences have two origins. First, there is mixing between the $SU(2)_L$ doublet and the flavon. Second, there is sizable mixing between the SM top-quark and the heavy fermion T.

Gluon fusion is the most important production channel of the SM Higgs boson at the LHC. In the NP model, the interaction between the SM-like Higgs boson and the gluon is mediated by both the SM top-quark and the heavy fermion T. Denoting the SM and the NP hgg interactions as

$$c_{hgg}^{SM} h G_{\mu\nu}^a G^{\mu\nu,a}, \quad c_{hgg}^{NP} h G_{\mu\nu}^a G^{\mu\nu,a}, \quad (35)$$

respectively, we have

$$\frac{c_{hgg}^{NP}}{c_{hgg}^{SM}} = \frac{\lambda v c_H}{\sqrt{2}} \left\{ \frac{c_L s_R}{m_t} - \frac{s_L c_R \tau_T \left[1 + (1 - \tau_T) f(\tau_T)\right]}{m_T \tau_t \left[1 + (1 - \tau_t) f(\tau_t)\right]} \right\}$$
$$- \frac{\lambda' v s_H}{\sqrt{2}} \left\{ \frac{s_L s_R}{m_t} + \frac{c_L c_R \tau_T \left[1 + (1 - \tau_T) f(\tau_T)\right]}{m_T \tau_t \left[1 + (1 - \tau_t) f(\tau_t)\right]} \right\}, \quad (36)$$

where $s_H(c_H) \equiv \sin\theta_H(\cos\theta_H)$, $\tau_i \equiv 4m_i^2/m_h^2$ and

$$f(\tau) = \begin{cases} \arcsin^2\left(\sqrt{1/\tau}\right), & \tau \geqslant 1, \\ -\frac{1}{4}\left[\log(\eta_+/\eta_-) - i\pi\right]^2, & \tau < 1, \end{cases} \quad (37)$$

where $\eta_\pm \equiv 1 \pm \sqrt{1-\tau}$. The ratio is nearly independent of λ, M and λ' in the 3σ fit region from EWPO. In the limit of large fermion mass ($m_{t,T} \gg m_h$), we obtain

$$\frac{c_{hgg}^{NP}}{c_{hgg}^{SM}} \to \frac{\lambda v c_H}{\sqrt{2}} \left(\frac{c_L s_R}{m_t} - \frac{s_L c_R}{m_T} \right)$$
$$- \frac{\lambda' v s_H}{\sqrt{2}} \left(\frac{s_L s_R}{m_t} + \frac{c_L c_R}{m_T} \right)$$
$$= c_H. \quad (38)$$

The $h\gamma\gamma$ interaction is also modified in the NP model. The contributions from the light fermions are highly suppressed by the fermion mass, so we consider only the contribution from t, T and $W^\pm$. Denoting the SM and the new physics (NP) $h\gamma\gamma$ interaction as

$$c_{h\gamma\gamma}^{SM} h F_{\mu\nu} F^{\mu\nu}, \quad c_{h\gamma\gamma}^{NP} h F_{\mu\nu} F^{\mu\nu}, \quad (39)$$

and

$$\kappa_g = \frac{c_{hgg}^{NP}}{c_{hgg}^{SM}}, \quad \kappa_\gamma = \frac{c_{h\gamma\gamma}^{NP}}{c_{h\gamma\gamma}^{SM}}, \quad (40)$$

we derive

$$\kappa_\gamma = \frac{N_c Q_f^2 A_{1/2} \kappa_g + c_H A_1}{N_c Q_f^2 A_{1/2} + A_1}, \quad (41)$$

where

$$A_{1/2} = \tau_t \left[1 + (1 - \tau_t) f(\tau_t)\right], \quad (42)$$
$$A_1 = -\frac{1}{2}\left[2 + 3\tau_W + 3\left(2\tau_W - \tau_W^2\right) f(\tau_W)\right], \quad (43)$$

$N_c = 3$, and $Q_f = 2/3$ are the color factor and charge of the top-quark. In the limit of large fermion mass,

$$\kappa_g = \kappa_\gamma = c_H \quad (44)$$

is a very good numerical approximation for this model.

Because Φ does not couple to the SM fermions except the top-quark, all of the other $h\bar{f}f$ coupling strengths are rescaled by a factor of c_H. Therefore the NP effects will not change the SM-like Higgs boson decay branching ratios, but they will change the production cross section. The gluon-gluon fusion channel, vector boson fusion (VBF) channel, and the vector boson associated production (VH) channel are all suppressed by a factor of c_H^2.

For the $h\bar{t}t$ interaction, the ratio between the coupling constant and the top-quark Yukawa coupling constant in the SM is

$$\frac{v s_R}{\sqrt{2} m_t} \left(\lambda c_H c_L - \lambda' s_H s_L\right). \quad (45)$$

It will deviate from c_H by a small amount, but the $\bar{t}th$ production channel has a much smaller cross section than the other three channels.

The results from a fit of the Higgs boson inclusive cross section $\mu = \sigma/\sigma_{SM}$ by the CMS collaboration [21] is

$$\mu = 0.80 \pm 0.14. \quad (46)$$

The result from the ATLAS collaboration

$$\mu = 1.30 \pm 0.12(\text{stat})^{+0.14}_{-0.11}(\text{sys}). \quad (47)$$

would exclude most of the parameter space of the NP model [32]. However, at the 3σ C.L., the region $s_H^2 < 0.2$ is still allowed.

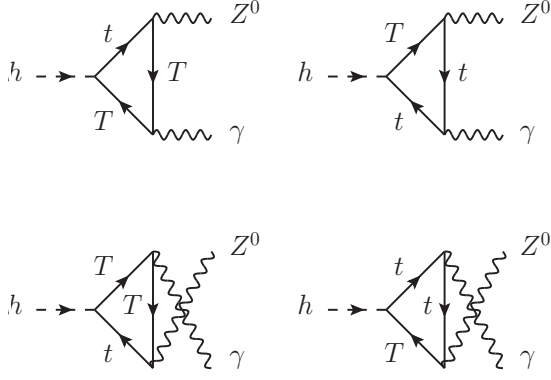Although the $h \to VV$ and $h \to f\bar{f}$ decay branching ratios are not changed in this NP model, owing to the

FIG. 3. Feynman diagrams for the additional contributions to $h \to Z^0\gamma$. Both t and T appear in the fermion loops.

universal rescaling factor c_H of hVV and $h\bar{f}f$ ($h \to t\bar{t}$ is forbidden because $m_h < 2m_t$), it is worth checking the $h \to Z^0\gamma$ decay branching ratio. In the NP model, there are additional contributions from both the T-loop and the $t-T$-loop (FIG. 3). The contributions from the t-loop and the T-loop can be read out from the rescaling of the SM amplitude. The additional contribution from the Feynman diagrams shown in FIG. 3 must be calculated independently. The effective operator can be written as $c_{hZ\gamma}hZ_{\mu\nu}F^{\mu\nu}$, where $Z_{\mu\nu}$ and $F_{\mu\nu}$ are the field strengths of the Z^0 and the electromagnetic field, respectively. The partial decay width of the Higgs boson is

$$\Gamma = \frac{|c_{hZ\gamma}|^2 m_h^3}{8\pi}\left(1 - \frac{m_Z^2}{m_h^2}\right)^3. \quad (48)$$

In the SM, there are contributions from the fermion loops and the $W^\pm$ loop. The contribution from the top-quark loop is

$$c_{hZ\gamma}^{SM,t} = \frac{\alpha g Q_t \left(8s_W^2 - 3\right)}{16\pi m_W s_W c_W}\left\{\frac{\tau_t \lambda_t}{\tau_t - \lambda_t}\right.$$
$$+2m_t^2 C_0\left(m_h^2, m_Z^2, 0, m_t^2, m_t^2, m_t^2\right)$$
$$+\frac{2m_t^2 \tau_t \lambda_t}{\tau_t - \lambda_t}C_0\left(m_h^2, m_Z^2, 0, m_t^2, m_t^2, m_t^2\right)$$
$$+\frac{\tau_t^2 \lambda_t}{(\tau_t - \lambda_t)^2}\left[B_0\left(m_Z^2, m_t^2, m_t^2\right)\right.$$
$$\left.\left.-B_0\left(m_h^2, m_t^2, m_t^2\right)\right]\right\}, \quad (49)$$

where $\lambda_t \equiv 4m_t^2/m_Z^2$, B_0 and C_0 are the standard Pasarino-Veltman functions. We use the $ht\bar{t}$ coupling constant $y_t = (gm_t)/(2m_W)$ in the SM. The contribu-

tions from the pure top and T loops in the NP case are

$$c_{hZ\gamma}^{NP,t} = \frac{\sqrt{2}m_W s_R \left(8s_W^2 - 3c_L^2\right)}{gm_t \left(8s_W^2 - 3\right)}$$
$$\times \left(\lambda c_L c_H - \lambda' s_L s_H\right)c_{hZ\gamma}^{SM,t}, \quad (50)$$
$$c_{hZ\gamma}^{NP,T} = -\frac{\sqrt{2}m_W c_R \left(8s_W^2 - 3s_L^2\right)}{gm_T \left(8s_W^2 - 3\right)}$$
$$\times \left(\lambda s_L c_H + \lambda' c_L s_H\right)c_{hZ\gamma}^{SM,t}\left(t \to T\right). \quad (51)$$

The new contributions from the $t - T$ mixing loops are

$$c_{hZ\gamma}^{NP,tT} = -\frac{3\alpha\lambda Q_t c_H c_L s_L}{4\sqrt{2}\pi s_W c_W \left(m_h^2 - m_Z^2\right)^2}\left\{m_T\left(m_h^2 - m_Z^2\right)\right.$$
$$\times \left[c_L c_R\left(m_h^2 - 2m_T^2 - m_Z^2\right) + 2m_t m_T s_L s_R\right]$$
$$\times C_0\left(m_h^2, m_Z^2, 0, m_T^2, m_t^2, m_T^2\right) - m_t\left(m_h^2 - m_Z^2\right)$$
$$\times \left[s_L s_R\left(m_h^2 - 2m_t^2 - m_Z^2\right) + 2m_t m_T c_L c_R\right]$$
$$\times C_0\left(m_h^2, m_Z^2, 0, m_t^2, m_T^2, m_t^2\right) - 2\left(m_h^2 - m_Z^2\right)$$
$$\times \left(m_T c_L c_R - m_t s_L s_R\right) - 2m_Z^2\left(m_T c_L c_R\right.$$
$$\left.-m_t s_L s_R\right)\left[B_0\left(m_h^2, m_t^2, m_T^2\right)\right.$$
$$\left.\left.-B_0\left(m_Z^2, m_t^2, m_T^2\right)\right]\right\}$$
$$+\frac{3\alpha\lambda' Q_t s_H c_L s_L}{4\sqrt{2}\pi s_W c_W \left(m_h^2 - m_Z^2\right)^2}\left\{m_T\left(m_h^2 - m_Z^2\right)\right.$$
$$\times \left[s_L c_R\left(m_h^2 - 2m_T^2 - m_Z^2\right) - 2m_t m_T c_L s_R\right]$$
$$\times C_0\left(m_h^2, m_Z^2, 0, m_T^2, m_t^2, m_T^2\right) + m_t\left(m_h^2 - m_Z^2\right)$$
$$\times \left[c_L s_R\left(m_h^2 - 2m_t^2 - m_Z^2\right) - 2m_t m_T s_L c_R\right]$$
$$\times C_0\left(m_h^2, m_Z^2, 0, m_t^2, m_T^2, m_t^2\right) - 2\left(m_h^2 - m_Z^2\right)$$
$$\times \left(m_T s_L c_R + m_t c_L s_R\right) - 2m_Z^2\left(m_T s_L c_R\right.$$
$$\left.+m_t c_L s_R\right)\left[B_0\left(m_h^2, m_t^2, m_T^2\right)\right.$$
$$\left.\left.-B_0\left(m_Z^2, m_t^2, m_T^2\right)\right]\right\}. \quad (52)$$

The analytic formulas of the Passarino-Veltman functions can be found in [33, 34]. The correction from NP is comparable to the contribution from the SM fermion loops. Because the partial width is not rescaled by just c_H^2 but has a more complicated behavior, the branching ratio is changed by the NP. We show the ratio between the Br $\left(h \to Z^0\gamma\right)$ in the NP and the SM in FIG. 4. As seen in FIG. 4, the NP contribution increases Br $\left(h \to Z^0\gamma\right)$. When the $\sin\theta_L$ and m_T parameters satisfy the SM EWPO at 3 σ C.L., the correction to Br $\left(h \to Z^0\gamma\right)$ is small.

Last but not least, an important question is how the SM Higgs pair-production cross section [35] is changed in this model of NP. There are two sources of change. The first is from flavon decay. The flavon can be produced singly at the LHC. If it decays into the hh final state with a sizable decay branching ratio, the hh cross section will be enhanced significantly owing to the resonance. The second source comes from corrections to the $ht\bar{t}$ and hhh

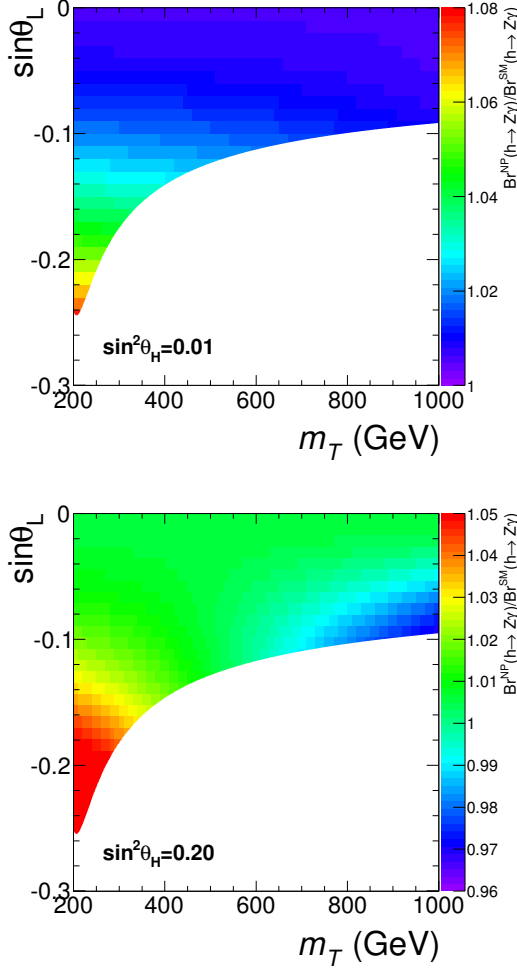NP model we have at large M

$$c_{hgg} = c_{hgg}^{SM} c_H, \tag{53}$$

$$
\begin{aligned}
c_{hhgg} = \frac{c_{hhgg}^{SM}}{2\left(m_T^2 - m_t^2\right)^2} &\left\{ c_H^2 \left[2\left(m_T^4 + m_t^4\right) \right.\right. \\
&\left. -2\lambda^2 v^2 \left(m_T^2 + m_t^2\right) + \lambda^4 v^4 \right] \\
&-2c_H s_H \sqrt{\left(2m_T^2 - \lambda^2 v^2\right)\left(\lambda^2 v^2 - 2m_t^2\right)} \\
&\times \left(\lambda^2 v^2 - m_T^2 - m_t^2\right)\frac{\lambda'}{\lambda} \\
&\left. + s_H^2 \left(2m_T^2 - \lambda^2 v^2\right)\left(\lambda^2 v^2 - 2m_t^2\right)\frac{\lambda'^2}{\lambda^2} \right\},
\end{aligned} \tag{54}
$$

where c_{hhgg} is the coupling constant of the interaction $hhG_{\mu\nu}^a G^{\mu\nu,a}$. In the allowed parameter space $\lambda v \to \sqrt{2} m_t + 0^+$,

$$c_{hhgg} = c_{hhgg}^{SM} c_H^2 \tag{55}$$

is therefore a very accurate approximation. We use this approximation in our numerical calculation. Moreover,

$$\lambda_{hhh} = \frac{m_h^2}{2v}\left(c_H^3 - s_H^3 \sqrt{\frac{\lambda_\Phi v^2}{m_\varphi^2 c_H^2 + m_h^2 s_H^2}} \right), \tag{56}$$

where λ_{hhh} is the trilinear coupling strength of the SM-like Higgs boson.

It was argued recently that a contribution from a higher dimensional operator such as $\left(H^\dagger H\right)\bar{Q}_L \tilde{H} t_R$ might be important in new physics models [40]. In the present model, such higher dimensional operators can be generated when we integrate out the heavy fermion and gauge boson degrees of freedom at the cutoff scale $\Lambda \gtrsim 10$ TeV (FIG. 5). These operators are suppressed
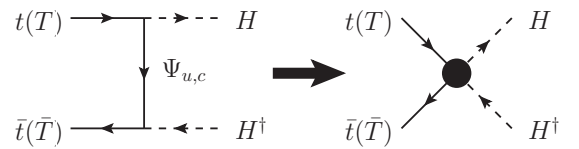

FIG. 5. The Feynman diagram by which the $\left(H^\dagger H\right)\bar{Q}_L \tilde{H} t_R$ operator can be generated. The $\Psi_{u,c}$ are the heavy fermion eigenstates of the first and the second generations in the UV completion of the flavor symmetry model with inverted hierarchy.

by the mass of $\Psi_{u,c}$, the heavy fermion eigenstates of the first and the second generations in the UV completion of the flavor symmetry model with inverted hierarchy, and also by a second power of the flavor changing interaction strength between the third and the first (or second) generation. Since the mass of $\Psi_{u,c}$ is of the order of $Mv/m_{c,u} \gtrsim 100$ TeV, the contribution from these operators will be small, and we do not include them in our calculation.

FIG. 4. The ratio between $\mathrm{Br}\left(h \to Z^0 \gamma\right)$ in the NP model and the SM is shown as a function of the mass of the heavy fermion m_T and the mixing angle of the left handed fermions s_L. We show the result in the region where the model can fit the EWPO at $3\,\sigma$ C.L.. We choose $m_\varphi = 300$ GeV and $\lambda_\Phi = 1.0$. In the upper panel, we choose $s_H^2 = 0.01$. In the lower panel, $s_H^2 = 0.20$.

vertices. We leave flavon production and decay to the next section but discuss the modifications of the vertices here.

According to the low-energy theorem [36–39], in this

We use the program HPAIR [41] to calculate the NLO cross section including the vertex corrections. In the pure SM case, $\sigma_{hh} = 34$ fb at 14 TeV. The result in the NP case is shown in FIG. 6. In most of the θ_H, m_φ space, the SM Higgs pair production cross section is nearly independent of the mass of the flavon for small λ_Φ. Without including flavon decays into hh, σ_{hh} is suppressed for large s_H^2.
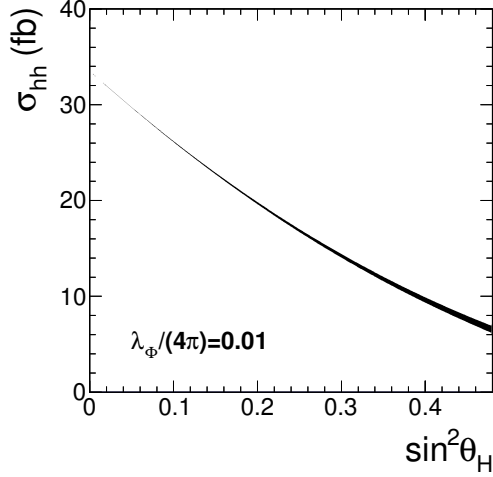
FIG. 6. The SM-like Higgs pair production cross section in the NP model (without the flavon resonance effect). We choose $\lambda_\Phi/(4\pi) = 0.01$ in the calculation.

To summarize this section, we investigated the production cross section and the decay properties of the SM-like Higgs boson h in the gauged flavor symmetry model with inverted hierarchy. We showed that the coupling strengths of most of the vertices are just rescaled by a factor c_H. We checked the loop induced interactions also. The hgg and $h\gamma\gamma$ vertices are rescaled by the factor c_H in the heavy fermion limit. The $hZ^0\gamma$ vertex deviates from the simple c_H rescaling, but the deviation is small. The inclusive Higgs production cross section is suppressed by a factor c_H^2, allowed by the LHC data at 7 and 8 TeV. The decay branching ratios are nearly unchanged relative to the SM since every sizable partial width is changed by an overall factor c_H^2. Finally, we computed the hh production cross section in this NP model (without the contribution from the flavon resonance decay).

V. FLAVON PHENOMENOLOGY AT THE LHC

In the previous section, we explored the influence of the NP model on SM-like Higgs boson physics at the LHC. In this section, we investigate searches for the flavon φ.[3]

---

[3] A study of flavon phenomenology in Froggatt-Nielsen models [42] can be found in [43, 44].

The flavon is produced dominantly through gluon fusion at the LHC. The effective interaction between φ and gluons is

$$c_{\varphi gg}\varphi G_{\mu\nu}^a G^{\mu\nu,a}, \qquad (57)$$

where

$$\frac{c_{\varphi gg}}{c_{hgg}^{SM}} = \frac{\lambda' v c_H}{\sqrt{2}} \left\{ \frac{s_L s_R}{m_t} + \frac{c_L c_R \tau_T [1 + (1 - \tau_T) f(\tau_T)]}{m_T \tau_t [1 + (1 - \tau_t) f(\tau_t)]} \right\}$$
$$- \frac{\lambda v s_H}{\sqrt{2}} \left\{ \frac{c_L s_R}{m_t} - \frac{s_L c_R \tau_T [1 + (1 - \tau_T) f(\tau_T)]}{m_T \tau_t [1 + (1 - \tau_t) f(\tau_t)]} \right\}. \qquad (58)$$

Here c_{hgg}^{SM} is the SM hgg effective coupling constant for a Higgs boson with the same mass as the flavon. When the flavon is heavy, the heavy fermion limit is not a good approximation (FIG. 7). In this work, we calculate the flavon production cross section using the full expression Eq. (58). A global fit of Higgs boson production cross sections at 7 and 8 TeV by the CMS collaboration, provides $s_H^2 \leqslant 0.62$ at 3σ C.L.[21]. According to the global fit by the ATLAS collaboration, s_H^2 should be smaller than 0.21 at 3σ C.L. [32].

In contrast to the gluon fusion case, the flavon cross sections in the VBF and vector boson associated production channels, where loop effects do not play a role, are just rescaled by a factor of s_H^2 relative to the Higgs boson cross sections.
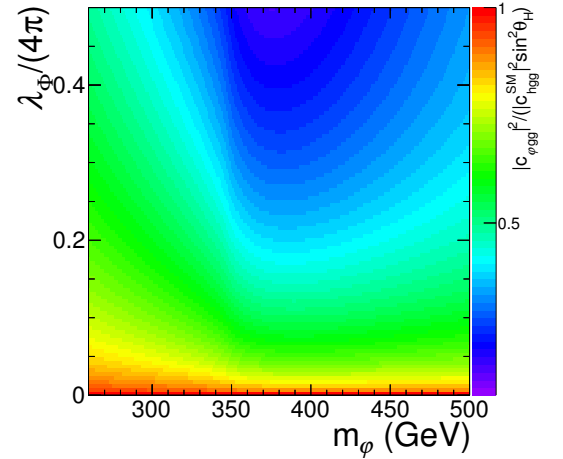

FIG. 7. The deviation of $|c_{\varphi gg}/c_{hgg}^{SM}|^2$ from the heavy fermion limit s_H^2 is plotted as a function of λ_Φ and the flavon mass m_φ.

The flavon has the same decay modes as the SM Higgs boson. For a light flavon ($m_\varphi < 2m_t$), the partial decay widths of the regular decay channels (except $\varphi \to gg, \gamma\gamma, \gamma Z$) are all rescaled by a factor of s_H^2 which will not affect the decay branching ratios of the flavon.

In addition, it is important to calculate the $\varphi \to hh$ decay width and, for a relatively heavy flavon ($2m_t <$

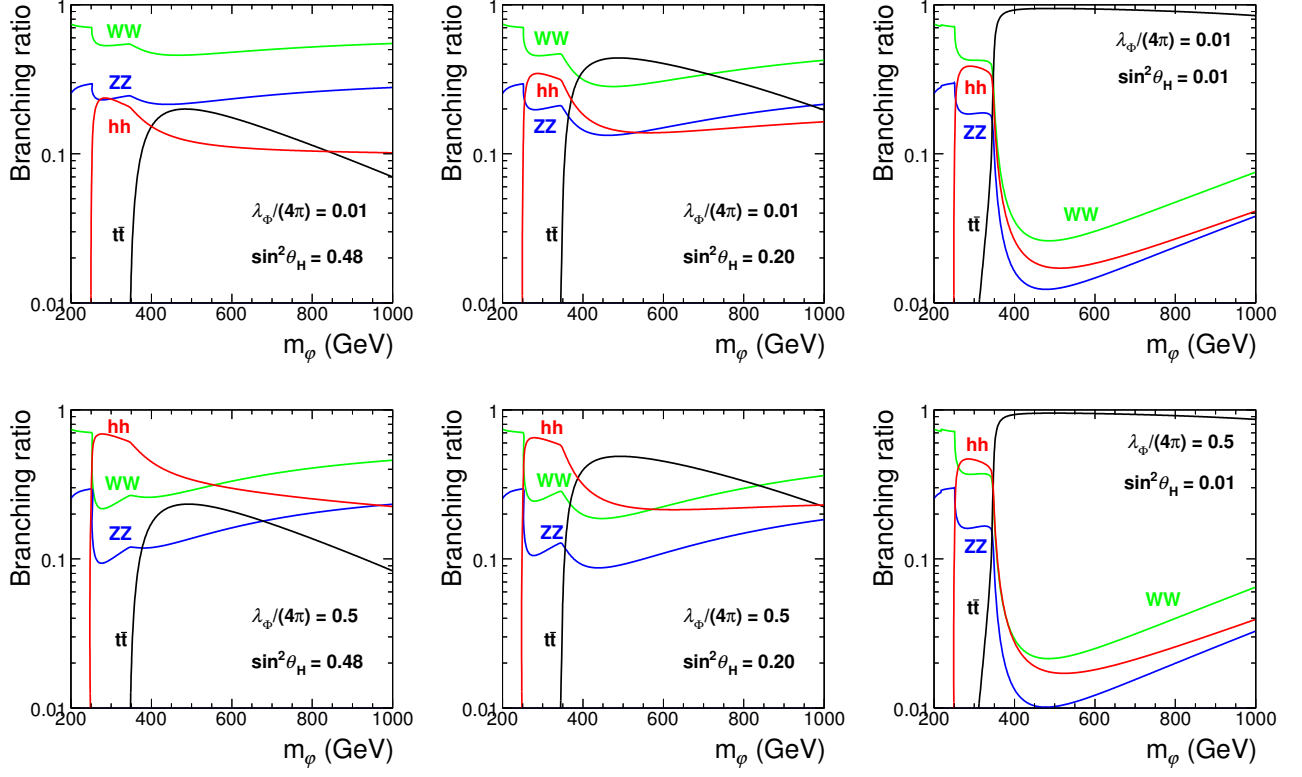FIG. 8. The decay branching ratios of the most important φ decay channels. Only the W^+W^-, Z^0Z^0, hh and $t\bar{t}$ channels are significant in φ decay. In this calculation, we choose $M = 2000$ GeV, and $\lambda = 1.1$.

$m_\varphi < m_t + m_T$), the $\varphi \to t\bar{t}$ decay width. For $\varphi \to hh$, we find

$$\Gamma\left(\varphi \to hh\right) = \frac{\lambda_{\varphi hh}^2 \beta_h}{8\pi m_\varphi}, \tag{59}$$

where $\beta_h \equiv \sqrt{1 - 4m_h^2/m_\varphi^2}$ and

$$\lambda_{\varphi hh} = \frac{\left(m_\varphi^2 + 2m_h^2\right)s_H c_H}{2v}$$
$$\times \left(c_H + s_H\sqrt{\frac{\lambda_\Phi v^2}{m_\varphi^2 c_H^2 + m_h^2 s_H^2}}\right). \tag{60}$$

In the small mixing limit ($s_H^2 \to 0$), we have

$$\lambda_{\varphi hh} \to \frac{m_\varphi^2 + 2m_h^2}{2v}s_H. \tag{61}$$

In particular, in the heavy flavon limit ($m_\varphi \gg m_h, m_Z$) with small s_H^2, we have $\Gamma\left(\varphi \to hh\right) = \Gamma\left(\varphi \to Z^0Z^0\right)$ which is a natural expectation of the equivalence theorem [45].

The contribution from the 3-body decay $\varphi \to hh^* \to$

$hf\bar{f}$ is [46]

$$\Gamma\left(\varphi \to hf\bar{f}\right) = \sum_f \frac{\lambda_{\varphi hh}^2 N_c m_f^2}{256\pi^3 m_\varphi v^2 \sqrt{z-1}}$$
$$\times \left[2\left(5z-4\right)\arctan\left(\frac{(z-4)\sqrt{z-1}}{4-3z}\right)\right.$$
$$\left. + (z-4)\sqrt{z-1}\left(4 + \log\frac{4}{z}\right)\right]. \tag{62}$$

It is numerically small ($z \equiv 4m_h^2/m_\varphi^2$).

We may calculate the partial width for $\varphi \to t^{(*)}\bar{t}^{(*)}$ (on-shell or off-shell top quarks) by rescaling the SM $h \to t^{(*)}\bar{t}^{(*)}$ with the factor

$$\frac{s_R^2 v^2}{2m_t^2}\left(\lambda c_H c_L - \lambda' s_H s_L\right)^2. \tag{63}$$

Since there is no s_H^2 suppression in the $\varphi t\bar{t}$ vertex, the flavon will decay into $t\bar{t}$ with a large branching ratio at small s_H if allowed by phase space. However, the flavon production cross section is highly suppressed by s_H^2 in this region. The signal will be hidden under the SM $t\bar{t}$ background making this signal for the flavon hard to find.

For a heavy flavon, as noted before, the heavy fermion limit is not a good approximation. We calculate the branching ratios of the loop-induced processes

$(\gamma\gamma, gg, Z^0\gamma)$ using the exact formula. The calculation is straightforward, but the result depends on all parameters. For $m_\varphi > 160$ GeV, the contribution from the loop induced channels is negligibly small, and the most important decay modes are $b\bar{b}, t\bar{t}, W^+W^-, Z^0Z^0$, and hh. These are the decay modes we must consider since we treat only $m_\varphi < m_T$ and $m_\varphi < 2m_{Z_T}$ in this work. The decay branching ratios for the dominant decay channels can be found in FIG. 8. For small s_H ($s_H^2 = 0.01$), $\varphi \to t\bar{t}$ dominates φ decay when the channel is open. This result arises because the $\varphi t\bar{t}$ interaction comes from the flavon-top interaction in Eq. 3.

In summary, $\varphi \to hh$ is an important decay channel of the flavon, and it might be used to discover the flavon at the LHC.

Flavon searches at the LHC can focus on the SM Higgs-like decay channels (Z^0Z^0, W^+W^-) and on the light Higgs boson pair decay channel. Although the SM Higgs-like decay channels of the flavon are suppressed by the presence of the hh decay channel, one should nevertheless check them carefully. In the remainder of this section, we examine constraints on the flavon from data at 7 and 8 TeV at the LHC and study flavon phenomenology at 14 TeV.

A. Limits from the 7 and 8 TeV LHC data

At 7 and 8 TeV, the strongest limit on the flavon is provided by the $Z^0Z^0 \to 2\ell2\ell'$ channel in heavy SM Higgs boson searches [47, 48]. The CMS collaboration also investigated the hh channel [49, 50]. For a heavy enough flavon, $t\bar{t}$ resonance searches may also constrain the parameters [51, 52]. However, the small production cross section makes this constraint weak. We do not discuss it here.

1. The $\varphi \to Z^0Z^0$ channel

The Z^0Z^0 channel has been examined by the ATLAS and CMS collaborations. ATLAS uses data corresponding to integrated luminosities of 4.6 fb^{-1} and 20.7 fb^{-1} at 7 TeV and 8 TeV, respectively [47] (the constraint on a heavy SM Higgs boson is from the 8 TeV data only). The CMS collaboration uses data corresponding to integrated luminosities of 5.1 fb^{-1} and 19.7 fb^{-1} at 7 TeV and 8 TeV, respectively [48]. We use these results to place constraints on the flavon.

For the ATLAS analysis, we use the gluon fusion channel because this channel is the dominant production channel for φ at the LHC. We use the expressions presented in this paper to rescale the Higgs boson production cross sections in [53] to get a NNLO QCD result. The numerical results are shown in FIG. 9 where we present the lower bound of the 2σ exclusion region of s_H^2 from heavy SM Higgs boson searches at 7 and 8 TeV as a function of the flavon self-iteraction parameter λ_Φ and its mass m_φ.
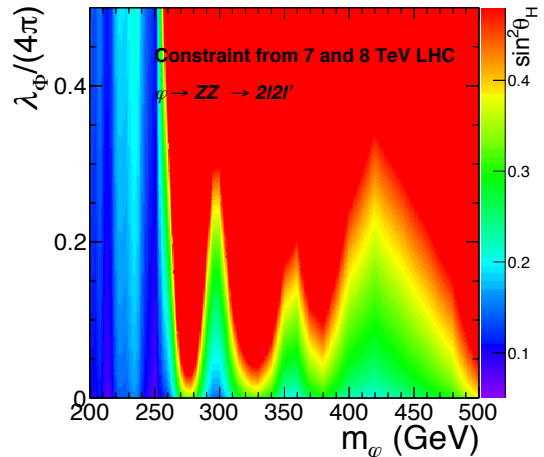

FIG. 9. The lower bound of the 2σ exclusion region of s_H^2 from the Z^0Z^0 channel heavy SM Higgs boson searches at 7 and 8 TeV is shown as a function of λ_Φ and m_φ. We choose $M = 2000$ GeV in this calculation. In the red region, the constraint from fitting the Higgs boson inclusive cross section is stronger. The peaks and valleys in the figure reflect the structure of the experimental exclusion bound.

In the blue region, values of s_H^2 above 0.2 are excluded at 2σ.

2. The $\varphi \to hh$ channel

The CMS collaboration searched for a heavy scalar (pseudo-scalar) decaying into hh (Z^0h) at 8 TeV with 19.5 fb^{-1} of data [49, 50]. Multilepton events with or without a diphoton and $b\bar{b}\gamma\gamma$ in the final state were used in those searches. This channel could be important for a flavon search when the $\varphi \to hh$ channel opens. However, with current luminosity, it does not yield a stronger constraint on NP than the SM Higgs global-fit. The ATLAS collaboration searched for a TeV-scale resonance decaying into hh at 8 TeV with 19.5 fb^{-1} of data using the $b\bar{b}b\bar{b}$ final state [54] and $b\bar{b}\gamma\gamma$ final state [55].

It might seem strange that the hh channel cannot provide a stronger constraint even when the Z^0Z^0 channel is highly suppressed, but it is understandable once we check the result carefully. The 2σ level lower bound on s_H^2 from the Z^0Z^0 channel is $0.1-0.2$. However, the upper bound on $\sigma(pp \to \varphi + X \to hh + X)$ is several picobarns, which is already above the SM heavy Higgs boson cross section in that mass region. Thus it cannot provide a constraint on s_H^2.

B. Searches for φ at 14 TeV

We investigate the possibility of discovering a flavon at 14 TeV with 100 fb^{-1} integrated luminosity.

1. Z^0Z^0 channel

There are simulations by the ATLAS collaboration [56] and the CMS collaboration [57] for this channel. We
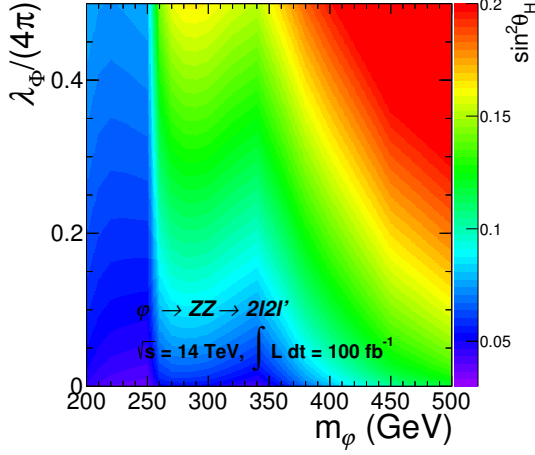

FIG. 10. The expected lower bound of the 2σ exclusion region of s_H^2 from searches for heavy scalar decays to Z^0Z^0 at the LHC at 14 TeV with 100 fb^{-1} integrated luminosity is shown as a function of λ_Φ and m_φ. We choose $M = 2000$ GeV in this calculation.

rescale their upper bounds to 100 fb^{-1} integrated luminosity by $\sqrt{\mathcal{L}_{\text{int}}/100\text{fb}^{-1}}$. The constraint from this channel is shown in FIG 10. When $m_\varphi < 2m_h$, it is evident from the left blue and green band in the figure that the Z^0Z^0 channel can provide a very strong constraint on the NP model (e.g., all s_H^2 greater than ~ 0.08 is excluded). When $m_\varphi > 2m_h$, the constraint on s_H^2 is at $\mathcal{O}\left(10^{-1}\right)$. In this region of s_H^2, the hh channel will be the dominant decay channel of φ.

2. hh channel

We focus on the $b\bar{b}\gamma\gamma$ channel and present the results of our detailed simulation of the signal and backgrounds. Efforts have been made to use this channel for new resonance searches, for example, see [58–61]. The $b\bar{b}\tau^+\tau^-$ channel [62] is also useful but we do not discuss it. The $b\bar{b}W^+W^-$ channel, which is useful when the final state SM Higgs bosons are boosted [63], is less important because the Higgs bosons are not highly boosted in our case. There are several irreducible SM backgrounds

$$\begin{aligned}
pp &\to b\bar{b}\gamma\gamma, \\
pp &\to Z^0 h \to b\bar{b}\gamma\gamma, \\
pp &\to Z^0\gamma\gamma \to b\bar{b}\gamma\gamma,
\end{aligned} \tag{64}$$

and reducible SM backgrounds

$$\begin{aligned}
pp &\to b\bar{b}jj \;\; (j \to \gamma), \\
pp &\to jj\gamma\gamma \;\; (j \to b), \\
pp &\to t\bar{t} \to bjj\bar{b}jj \;\; (j \to \gamma), \\
pp &\to t\bar{t}h \to b\ell^+\nu\bar{b}\ell^-\bar{\nu}\gamma\gamma \;\; \left(\ell^\pm \text{ missed}\right).
\end{aligned} \tag{65}$$

We generate the signal and background events at the parton level using MadGraph 5 [64, 65] with CTEQ6L1 parton distribution functions (PDF) [66]. For signal events, we generate $pp \to \varphi + \text{n}j$ to n=1. All of the parton level signal and the background events are showered using Pythia6.4 [67]. The MLM matching scheme [68] is used to avoid double counting. Detector effects are mimicked with PGS4 [69]. Jets are defined in the events with the anti-k_T algorithm, with $R = 0.4$. The cross section of the Z^0h process is reweighted to the value suggested by the LHC Higgs Cross Section Working Group in which the NNLO QCD and NLO EW corrections have been included [53]. The $Z^0\gamma\gamma$ and $b\bar{b}\gamma\gamma$ cross sections are reweighted to the NLO QCD results by mutiplication with a simple K-factor [70–72]. The jet fake rate is rescaled by [73]

$$\epsilon\left(p_T\right)_{j\to\gamma} = 9.3 \times 10^{-3} \times \exp\left(-\frac{p_T}{27.5 \text{ GeV}}\right). \tag{66}$$

We require the events to have at least two hard isolated photons in the central region, which means

$$p_T^\gamma > 20\text{GeV}, \quad |\eta^\gamma| < 2.0, \tag{67}$$

and no hard jet or charged lepton in the $\Delta R = 0.4$ region around the photon. The events should also have at least two hard b-tagged jets with

$$p_T^j > 40 \text{ GeV}, \quad \left|\eta^j\right| < 2.0. \tag{68}$$

The average b-tagging efficiency is reweighted to 70% [73] in this analysis. The light flavor (g, u, d, s) and charm quark mis-tag rates are chosen to be 3.9% and 25.7%, respectively. To suppress the SM $t\bar{t}h$ background, we reject events which contain hard isolated charged leptons with

$$p_T^\ell > 20 \text{ GeV}, \quad \left|\eta^\ell\right| < 2.5, \quad \left(I_{iso} < 0.1 \text{ for } \mu^\pm\right) \tag{69}$$

and events which have a large missing transverse energy

$$\not{E}_{\text{T}} > 30 \text{ GeV}. \tag{70}$$

We require signal events to satisfy hard cuts designed for the Higgs boson pair signal. The leading and subleading photon in the events should satisfy

$$|m_{\gamma\gamma} - 125.4 \text{ GeV}| < \Delta m_{h,\text{cut}}^{\gamma\gamma}. \tag{71}$$

The transverse momentum of the leading and of the subleading photon should satisfy

$$p_T^{\gamma_1} > p_{T,\text{cut}}^{\gamma_1}, \quad p_T^{\gamma_2} > p_{T,\text{cut}}^{\gamma_2}. \tag{72}$$
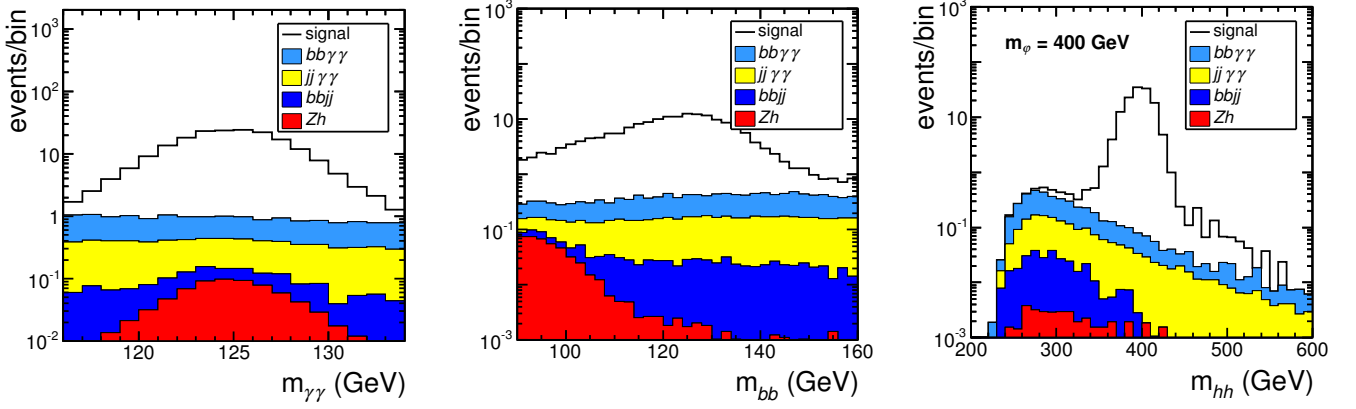
FIG. 11. The reconstructed diphoton, $b\bar{b}$, and hh mass distributions are shown at 14 TeV with 100 fb^{-1} integrated luminosity. We choose m_φ =400 GeV. The total cross section is rescaled to the value of the SM like Higgs boson with the same mass. The decay branching ratio Br $(\varphi \to hh)$ is set to be 100%. In the left and middle panels, the events passed the all of the cuts except the $\gamma\gamma$ and bb invariant mass cuts. In the right panel, the events pass all of the cuts. Note that the horizontal scale differs in the three distributions.

We require the leading and subleading b-tagged jets to satisfy

$$|m_{bb} - 125.4 \text{ GeV}| < \Delta m_{h,\text{cut}}^{bb}. \qquad (73)$$

$\delta\phi_{\gamma b}$, the smallest of $\Delta\phi_{\gamma_1 b_1}, \Delta\phi_{\gamma_1 b_2}, \Delta\phi_{\gamma_2 b_1}, \Delta\phi_{\gamma_2 b_2}$ (the differences between the azimuthal angles of the objects) should be less than $\Delta\phi_{\gamma b}$.

The energy resolutions of b-jets and photons are obtained from the $Z^0 b \to \mu^+\mu^- b$ and the $Z^0\gamma \to \mu^+\mu^-\gamma$ processes. After including the energy resolution, we can reconstruct the invariant mass peak of the flavon.

The values of the $p_{T,\text{cut}}^{\gamma_1}, p_{T,\text{cut}}^{\gamma_1}, \Delta m_{h,\text{cut}}^{bb}, \Delta m_{h,\text{cut}}^{\gamma\gamma}, \Delta\phi_{\gamma b}$ and the invariant mass window of the hh system are chosen with the mass of the flavon to get a maximal signal significance (TABLE II and III). When the mass of the flavon increases, a larger leading photon p_T cut will give larger significance because the final state Higgs boson is more boosted. Such a large leading photon p_T cut will suppress the SM background so that we can release the diphoton invariant mass cut to include more signal events.

For a flavon whose mass is relatively small, the b-jets (diphoton) from the Higgs boson decay are not too collinear. In such a case, a $\Delta\phi_{\gamma b}$ cut can suppress the QCD background from $q\bar{q} \to b\bar{b}\gamma\gamma$ where the b-jets are from a virtual gluon splitting and the photons are from the initial state radiation (ISR). This is the reason a small $\Delta\phi_{\gamma b}$ can give larger significance for light flavons. For the $m_\varphi \sim 280-290$ GeV region, the production cross section drops and the $\Delta\phi_{\gamma b}$ cut will remove many signal events and not be helpful for increasing significance if we cannot increase the p_T cuts. Thanks to the "bump" structure in the $gg \to \varphi$ cross section around $m_\varphi \sim 2m_t$, there is a larger cross section for that region of flavon mass. More signal events allow us to use harder p_T cuts and the $\Delta\phi_{\gamma b}$ cut. For a heavy flavon, the two b-jets (diphoton) are more and more collinear and $\Delta\phi_{\gamma b}$ is no longer

a good cut. In FIG. 11, we show the results for the reconstructed diphoton, $b\bar{b}$, and hh mass distributions using events which satisfy all the cuts. The resonance signal is very clear. The dominant background is $b\bar{b}\gamma\gamma$, and the other backgrounds are numerically small. The diphoton resonance is extremely clear, and the $b\bar{b}$ peak is wide owing to the larger energy smearing of jets.

After a scan over the mass of the flavon, we show expected limits from the search for the $\varphi \to hh \to b\bar{b}\gamma\gamma$ signal at 14 TeV with 100 fb^{-1} in FIG. 12. The number of events is small so we calculate the 2σ exclusion bound using

$$\sqrt{-2\left[n_b \ln\left(\frac{n_s + n_b}{n_b}\right) - n_s\right]} = 2, \qquad (74)$$

where n_s and n_b are the numbers of signal and background events, respectively [74]. The 5σ discovery significance is calculated using

$$\sqrt{-2\left[(n_b + n_s)\ln\left(\frac{n_b}{n_s + n_b}\right) + n_s\right]} = 5. \qquad (75)$$

The limits shown in FIG. 12 can be translated into a constraint on the NP parameters.

Combining the results from the SM-like heavy Higgs boson search for $\varphi \to Z^0 Z^0$ and the $\varphi \to hh \to b\bar{b}\gamma\gamma$ search at 14 TeV with 100 fb^{-1} integrated luminosity, we show the constraint on s_H^2 in FIG. 13. The combined 5σ discovery significance is shown in FIG. 14. In FIG. 13, the search for the $\varphi \to hh \to b\bar{b}\gamma\gamma$ signal gives a stronger constraint in the cross-hatched region. This signal can give a stronger constraint in the large λ_Φ region when the $\varphi \to hh$ channel opens. This figure shows that a strong constraint on the neutral scalar φ can be obtained with a combination of the two channels.

TABLE II. The combination of cuts which gives the largest significance for excluding the flavon with different mass.

Exclusion	$p_{T,\text{cut}}^{\gamma_1}$	$p_{T,\text{cut}}^{\gamma_2}$	$\Delta m_{h,\text{cut}}^{\gamma\gamma}$	$\Delta m_{h,\text{cut}}^{bb}$	$\Delta\phi_{\gamma b}$	m_{hh} window
$m_\varphi = 260$ GeV	30 GeV	20 GeV	3.5 GeV	20 GeV	0.5π	230 GeV $\sim$ 280 GeV
$m_\varphi = 270$ GeV	35 GeV	20 GeV	3.5 GeV	20 GeV	0.5π	245 GeV $\sim$ 295 GeV
$m_\varphi = 280$ GeV	35 GeV	20 GeV	3.5 GeV	15 GeV	π	265 GeV $\sim$ 300 GeV
$m_\varphi = 290$ GeV	30 GeV	20 GeV	3.5 GeV	15 GeV	π	275 GeV $\sim$ 310 GeV
$m_\varphi = 300$ GeV	35 GeV	20 GeV	4.0 GeV	15 GeV	0.7π	280 GeV $\sim$ 325 GeV
$m_\varphi = 320$ GeV	40 GeV	20 GeV	4.0 GeV	15 GeV	0.7π	300 GeV $\sim$ 345 GeV
$m_\varphi = 340$ GeV	45 GeV	20 GeV	4.0 GeV	15 GeV	0.8π	320 GeV $\sim$ 365 GeV
$m_\varphi = 360$ GeV	45 GeV	20 GeV	5.5 GeV	15 GeV	π	340 GeV $\sim$ 385 GeV
$m_\varphi = 380$ GeV	40 GeV	20 GeV	5.0 GeV	15 GeV	π	355 GeV $\sim$ 405 GeV
$m_\varphi = 400$ GeV	50 GeV	25 GeV	5.5 GeV	20 GeV	π	370 GeV $\sim$ 435 GeV
$m_\varphi = 450$ GeV	50 GeV	25 GeV	6.5 GeV	20 GeV	π	420 GeV $\sim$ 485 GeV
$m_\varphi = 500$ GeV	45 GeV	20 GeV	7.5 GeV	20 GeV	π	465 GeV $\sim$ 535 GeV
$m_\varphi = 550$ GeV	45 GeV	20 GeV	8.0 GeV	20 GeV	π	510 GeV $\sim$ 585 GeV
$m_\varphi = 600$ GeV	50 GeV	25 GeV	8.0 GeV	25 GeV	π	555 GeV $\sim$ 640 GeV

TABLE III. The combination of cuts which gives the largest significance for discovering the flavon with different mass.

Discovery	$p_{T,\text{cut}}^{\gamma_1}$	$p_{T,\text{cut}}^{\gamma_2}$	$\Delta m_{h,\text{cut}}^{\gamma\gamma}$	$\Delta m_{h,\text{cut}}^{bb}$	$\Delta\phi_{\gamma b}$	m_{hh} window
$m_\varphi = 260$ GeV	30 GeV	20 GeV	3.5 GeV	20 GeV	0.5π	230 GeV $\sim$ 280 GeV
$m_\varphi = 270$ GeV	35 GeV	20 GeV	3.5 GeV	20 GeV	0.5π	245 GeV $\sim$ 295 GeV
$m_\varphi = 280$ GeV	30 GeV	20 GeV	3.5 GeV	15 GeV	π	265 GeV $\sim$ 300 GeV
$m_\varphi = 290$ GeV	30 GeV	20 GeV	3.5 GeV	15 GeV	π	275 GeV $\sim$ 310 GeV
$m_\varphi = 300$ GeV	35 GeV	20 GeV	3.5 GeV	15 GeV	0.7π	285 GeV $\sim$ 320 GeV
$m_\varphi = 320$ GeV	45 GeV	20 GeV	4.0 GeV	15 GeV	0.7π	300 GeV $\sim$ 345 GeV
$m_\varphi = 340$ GeV	45 GeV	20 GeV	4.0 GeV	15 GeV	0.8π	320 GeV $\sim$ 365 GeV
$m_\varphi = 360$ GeV	45 GeV	25 GeV	5.5 GeV	15 GeV	0.8π	340 GeV $\sim$ 385 GeV
$m_\varphi = 380$ GeV	50 GeV	25 GeV	5.0 GeV	15 GeV	0.8π	360 GeV $\sim$ 405 GeV
$m_\varphi = 400$ GeV	50 GeV	25 GeV	5.5 GeV	15 GeV	π	380 GeV $\sim$ 425 GeV
$m_\varphi = 450$ GeV	50 GeV	25 GeV	6.5 GeV	15 GeV	π	425 GeV $\sim$ 475 GeV
$m_\varphi = 500$ GeV	45 GeV	20 GeV	6.5 GeV	15 GeV	π	475 GeV $\sim$ 530 GeV
$m_\varphi = 550$ GeV	45 GeV	25 GeV	7.5 GeV	15 GeV	π	515 GeV $\sim$ 580 GeV
$m_\varphi = 600$ GeV	25 GeV	25 GeV	7.0 GeV	15 GeV	π	565 GeV $\sim$ 640 GeV

In this section, we investigated flavon phenomenology at the LHC in detail. We first examined the decay branching ratios and the production cross section of the flavon φ. The dominant decay channels are W^+W^-, Z^0Z^0, hh and $t\bar{t}$. We checked the limits on the flavon from heavy Higgs boson searches at 7 and 8 TeV. The hh signal was simulated in detail at 14 TeV. We showed that in some parts of parameter space the search for a hh signal yields a stronger constraint on the NP model than the Z^0Z^0 channel. Finally, we presented a combined result using the $hh \to 2b2\gamma$ and the $Z^0Z^0 \to 2\ell2\ell'$ channels.

VI. CONCLUSIONS

This paper has investigated a model of physics beyond the SM in which there is a new scalar, a flavon, a new heavy fermion associated with the SM top-quark, and a new neutral flavor gauge boson. This model arises as the low-energy limit of a theory of gauged flavor symmetry with an inverted hierarchy, giving a simplified model with spontaneous breaking of flavor symmetry. This model may be considered independently of its origin from the inverted hierarchy, as a model that could result from other physics and be interesting in its own right. The flavon mixes with the SM Higgs boson, and the heavy fermion
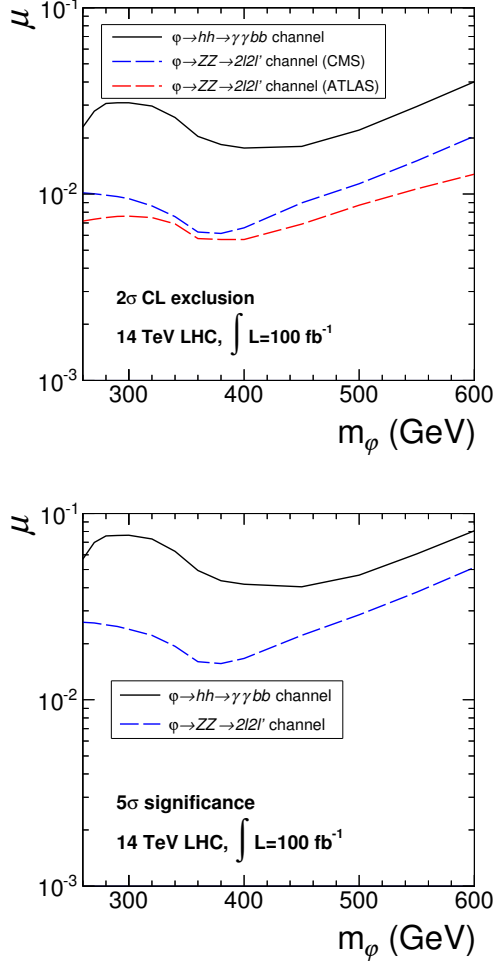
FIG. 12. The 2σ C.L. exclusion bound and the 5σ C.L. observation bound of the flavon production strength μ from the $pp \to \varphi \to hhX \to b\bar{b}\gamma\gamma X$ and the $pp \to \varphi \to ZZX \to 2\ell 2\ell'$ channels. $\mu \equiv \sigma\left(pp \to \varphi \to ZZ\right)/\sigma\left(pp \to H\right)$ for the ZZ channel and $\mu \equiv \sigma\left(pp \to \varphi \to hh\right)/\sigma\left(pp \to H\right)$ for the hh channel. The region above the curves will be excluded (discovered) at 2σ (5σ) C.L..

FIG. 13. Combination of the 2σ exclusion region of s_H^2 results for the $\varphi \to Z^0 Z^0 \to 2\ell 2\ell'$ search and the $\varphi \to hh \to b\bar{b}\gamma\gamma$ search. In the upper part of the figure, in the irregularly shaped region above the broad-dashed line, the $\varphi \to hh \to b\bar{b}\gamma\gamma$ search yields a stronger constraint.

FIG. 14. The 5σ discovery significance of the required value of s_H^2 from a combination of the $\varphi \to Z^0 Z^0 \to 2\ell 2\ell'$ search and the $\varphi \to hh \to b\bar{b}\gamma\gamma$ search. In the upper part of the figure, in the irregularly shaped region above the broad-dashed line, the $\varphi \to hh \to b\bar{b}\gamma\gamma$ process is more sensitive to the NP model.

alters the production and decay properties of the Higgs boson at the LHC, all in ways that are consistent with data at current levels of precision. The flavon and the heavy fermion might appear at the hundreds of GeV to the TeV scale. There is a sizable allowed parameter space in which existing constraints from electroweak precision observables and flavor physics are satisfied.

The mixing of the flavon, which is a gauge singlet scalar under the SM, with the $SU(2)_L$ doublet Higgs field produces two notable effects. First, its influence on Higgs boson physics could be examined with more precise measurements of the SM Higgs-like scalar at 125 GeV discovered recently at the LHC. Second, the mixing makes it possible to produce and detect the flavon at the LHC.

In this NP model, the production cross section of the SM-like Higgs boson at the LHC is suppressed by a factor
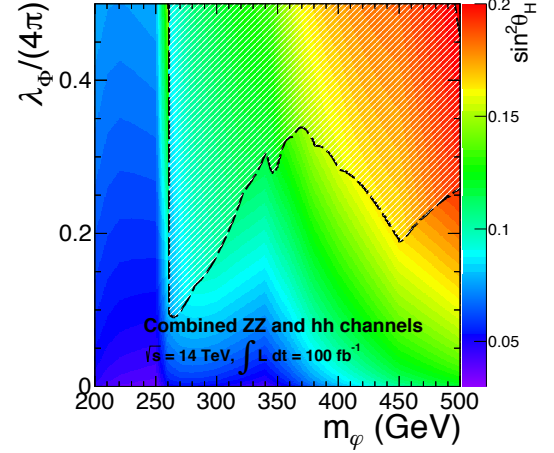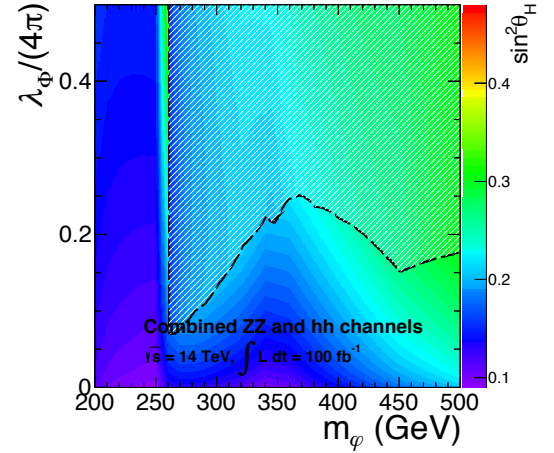
$\cos^2 \theta_H$, where θ_H is the mixing angle between the Higgs boson and the flavon. However, neither mixing nor the triangle loop from the heavy fermion change the Higgs boson decay branching ratios significantly. The $h \to Z^0\gamma$ decay channel is an exception. With large mixing which is still allowed at the 3σ level, the branching ratio of this channel can be increased by about 5%. It is not an easy task to measure this branching ratio precisely at the LHC, but it would be possible to check the modification of the $hZ^0\gamma$ vertex at a future Higgs Factory.

The possibility to search for the flavon at the LHC

is explored in detail in the paper. Generally, the mixing between an exotic scalar field φ and the SM Higgs field can be generated from $\mathcal{O}\left(\Phi\right)\left(H^\dagger H\right)$, where $\mathcal{O}\left(\Phi\right)$ is some operator constructed from Φ. As long as the scalar interacts with the SM sector, this interaction will arise from loop corrections even if forbidden artificially at tree-level. The φhh vertex usually appears once there is $\varphi - h$ mixing, and a NP heavy scalar boson which can decay into a SM Higgs-pair will also decay via the SM Higgs boson decay modes. This is also the case in this flavor symmetry model where the flavon decays to a SM Higgs-pair, $\varphi \to hh$, as well as through the SM Higgs boson decay modes.

We investigated the $\varphi \to Z^0 Z^0$ discovery channel. At 7 and 8 TeV at the LHC, the $Z^0 Z^0$ channel will give a stronger constraint than $\varphi \to hh$ owing to limitations of integrated luminosity. The large mixing required to get a large enough cross section is excluded by the global-fit of the Higgs boson inclusive cross section. At 14 TeV with 100 fb^{-1} integrated luminosity, we showed that the small mixing region can be reached where the $Z^0 Z^0$ decay channel is highly suppressed. In this region of the parameter space, the $\varphi \to hh$ signal is more important for discovery. Our result can be used to discover or exclude not only the flavon, but also singlet scalars in other models which can be produced through gluon fusion and decay into a Higgs pair [18, 19, 31, 75].

The SM Higgs pair production cross section is changed in this model of NP. The flavon can be produced singly at the LHC. If it decays into the hh final state with a sizable decay branching ratio, the hh cross section will be enhanced significantly by this resonance effect. A second source of change comes from corrections to the $h t \bar{t}$ and hhh vertices. These corrections generally reduce the SM Higgs pair rate as shown in FIG. 6.

In this work, we investigate the case $m_T > m_\varphi$ in which the new heavy fermion is more massive than the flavon. Such a heavy fermion has special decay modes and signals at the LHC. A relatively heavy flavon and the new massive vector boson $Z_{T\mu}$ might produce a four-top signal at the LHC, which is a potential discovery channel for these states. A study of the heavy fermion phenomenology and the top-philic vector boson phenomenology is left for another paper [76].

[1] G. Aad et al. (ATLAS Collaboration), Phys.Lett. **B716**, 1 (2012), arXiv:1207.7214.

[2] S. Chatrchyan et al. (CMS Collaboration), Phys.Lett. **B716**, 30 (2012), arXiv:1207.7235.

[3] N. Cabibbo, Phys.Rev.Lett. **10**, 531 (1963).

[4] M. Kobayashi and T. Maskawa, Prog.Theor.Phys. **49**, 652 (1973).

[5] G. D'Ambrosio, G. Giudice, G. Isidori, and A. Strumia, Nucl.Phys. **B645**, 155 (2002), arXiv:hep-ph/0207036.

[6] M. Leurer, Y. Nir, and N. Seiberg, Nucl.Phys. **B398**, 319 (1993), arXiv:hep-ph/9212278.

[7] M. Leurer, Y. Nir, and N. Seiberg, Nucl.Phys. **B420**, 468 (1994), arXiv:hep-ph/9310320.

[8] R. Zwicky and T. Fischbacher, Phys.Rev. **D80**, 076009 (2009), arXiv:0908.4182.

[9] S. Sun, D. B. Kaplan, and A. E. Nelson, Phys.Rev. **D87**, 125036 (2013), 1303.1811.

[10] Z. Berezhiani and J. Chkareuli, Sov.J.Nucl.Phys. **37**, 618 (1983).

[11] Z. Berezhiani, Phys.Lett. **B129**, 99 (1983).

[12] Z. Berezhiani and M. Y. Khlopov, Sov.J.Nucl.Phys. **51**, 739 (1990).

[13] B. Grinstein, M. Redi, and G. Villadoro, JHEP **1011**, 067 (2010), arXiv:1009.2049.

[14] T. Feldmann, JHEP **1104**, 043 (2011), arXiv:1010.2116.

[15] G. Krnjaic and D. Stolarski, JHEP **1304**, 064 (2013), arXiv:1212.4860.

[16] A. J. Buras, M. V. Carlucci, L. Merlo, and E. Stamou, JHEP **1203**, 088 (2012), arXiv:1112.4477.

[17] T. Feldmann, M. Jung, and T. Mannel, Phys.Rev. **D80**, 033003 (2009), arXiv:0906.1523.

[18] M.-L. Xiao and J.-H. Yu (2014), arXiv:1404.0681.

[19] H.-J. He and Z.-Z. Xianyu (2014), arXiv:1405.7331.

[20] S. Alekhin, A. Djouadi, and S. Moch, Phys.Lett. **B716**, 214 (2012), arXiv:1207.0980.

[21] Tech. Rep. CMS-PAS-HIG-13-005, CERN, Geneva (2013).

[22] G. Aad et al. (ATLAS Collaboration) (2014), arXiv:1406.3827.

[23] C.-W. Chiang, J. Jiang, T. Li, and Y.-R. Wang, JHEP **0712**, 001 (2007), arXiv:0710.1268.

[24] S.-L. Chen and N. Okada, Phys.Lett. **B669**, 34 (2008), arXiv:0808.0331.

[25] C. Jackson, G. Servant, G. Shaughnessy, T. M. Tait, and M. Taoso, JCAP **1004**, 004 (2010), arXiv:0912.0004.

[26] K. Hsieh, K. Schmitz, J.-H. Yu, and C.-P. Yuan, Phys.Rev. **D82**, 035011 (2010), arXiv:1003.3482.

[27] E. L. Berger, Q.-H. Cao, J.-H. Yu, and C.-P. Yuan, Phys.Rev. **D84**, 095026 (2011), arXiv:1108.3613.

[28] C. Han, A. Kobakhidze, N. Liu, L. Wu, and B. Yang (2014), 1405.1498.

[29] M. E. Peskin and T. Takeuchi, Phys.Rev.Lett. **65**, 964 (1990).

[30] M. Baak, M. Goebel, J. Haller, A. Hoecker, D. Kennedy, et al., Eur.Phys.J. **C72**, 2205 (2012), arXiv:1209.2716.

[31] V. Barger, P. Langacker, M. McCaskey, M. J. Ramsey-Musolf, and G. Shaughnessy, Phys.Rev. **D77**, 035005 (2008), arXiv:0706.4311.

[32] Tech. Rep. ATLAS-CONF-2014-009, CERN, Geneva (2014).

[33] G. 't Hooft and M. Veltman, Nucl.Phys. **B153**, 365 (1979).

[34] G. Passarino and M. Veltman, Nucl.Phys. **B160**, 151 (1979).

[35] D. Y. Shao, C. S. Li, H. T. Li, and J. Wang, JHEP **1307**, 169 (2013), arXiv:1301.1245.

[36] J. R. Ellis, M. K. Gaillard, and D. V. Nanopoulos, Nucl.Phys. **B106**, 292 (1976).

[37] M. A. Shifman, A. Vainshtein, M. Voloshin, and V. I. Zakharov, Sov.J.Nucl.Phys. **30**, 711 (1979).

[38] B. A. Kniehl and M. Spira, Z.Phys. **C69**, 77 (1995), arXiv:hep-ph/9505225.

[39] M. Gillioz, R. Grober, C. Grojean, M. Muhlleitner, and E. Salvioni, JHEP **1210**, 004 (2012), arXiv:1206.7120.

[40] C.-R. Chen and I. Low (2014), arXiv:1405.7040.

[41] M. Spira (2014), URL `http://tiger.web.psi.ch/proglist.html`.

[42] C. Froggatt and H. B. Nielsen, Nucl.Phys. **B147**, 277 (1979).

[43] K. Tsumura and L. Velasco-Sevilla, Phys.Rev. **D81**, 036012 (2010), 0911.2149.

[44] J. L. Diaz-Cruz (2014), 1405.0990.

[45] J. M. Cornwall, D. N. Levin, and G. Tiktopoulos, Phys.Rev. **D10**, 1145 (1974).

[46] A. Djouadi, J. Kalinowski, and P. Zerwas, Z.Phys. **C70**, 435 (1996), arXiv:hep-ph/9511342.

[47] Tech. Rep. ATLAS-CONF-2013-013, CERN, Geneva (2013).

[48] S. Chatrchyan et al. (CMS Collaboration) (2013), arXiv:1312.5353.

[49] Tech. Rep. CMS-PAS-HIG-13-025, CERN, Geneva (2013).

[50] Tech. Rep. CMS-PAS-HIG-13-032, CERN, Geneva (2013).

[51] Tech. Rep. ATLAS-CONF-2013-052, CERN, Geneva (2013).

[52] S. Chatrchyan et al. (CMS Collaboration) (2013), arXiv:1309.2030.

[53] S. Dittmaier et al. (LHC Higgs Cross Section Working Group) (2011), arXiv:1101.0593.

[54] Tech. Rep. ATLAS-CONF-2014-005, CERN, Geneva (2014).

[55] G. Aad et al. (ATLAS Collaboration) (2014), arXiv:1406.5053.

[56] Tech. Rep. ATLAS-PHYS-PUB-2013-016, CERN, Geneva (2013).

[57] Tech. Rep. CMS-PAS-FTR-13-024, CERN, Geneva (2013).

[58] N. Craig, J. Galloway, and S. Thomas (2013), arXiv:1305.2424.

[59] J. Liu, X.-P. Wang, and S.-h. Zhu (2013), arXiv:1310.3634.

[60] N. Chen, C. Du, Y. Fang, and L.-C. Lü (2013), arXiv:1312.7212.

[61] N. Kumar and S. P. Martin (2014), arXiv:1404.0996.

[62] J. M. No and M. Ramsey-Musolf (2013), arXiv:1310.6035.

[63] A. Papaefstathiou, L. L. Yang, and J. Zurita, Phys.Rev. **D87**, 011301 (2013), arXiv:1209.1489.

[64] J. Alwall, M. Herquet, F. Maltoni, O. Mattelaer, and T. Stelzer, JHEP **1106**, 128 (2011), arXiv:1106.0522.

[65] J. Alwall, R. Frederix, S. Frixione, V. Hirschi, F. Maltoni,

et al. (2014), arXiv:1405.0301.

[66] J. Pumplin, D. Stump, J. Huston, H. Lai, P. M. Nadolsky, et al., JHEP **0207**, 012 (2002), arXiv:hep-ph/0201195.

[67] T. Sjostrand, S. Mrenna, and P. Z. Skands, JHEP **0605**, 026 (2006), arXiv:hep-ph/0603175.

[68] M. L. Mangano, M. Moretti, F. Piccinini, and M. Treccani, J. High Energy Phys. **0701**, 013 (2007), arXiv:hep-ph/0611129.

[69] J. Conway et al. (2013), URL `http://www.physics.ucdavis.edu/~conway/research/software/pgs/pgs4-olympics.htm`.

[70] G. Bozzi, F. Campanario, M. Rauch, and D. Zeppenfeld, Phys.Rev. **D84**, 074028 (2011), arXiv:1107.3149.

[71] T. Gehrmann, N. Greiner, and G. Heinrich (2013), arXiv:1311.4754.

[72] Z. Bern, L. J. Dixon, F. Febres Cordero, S. Hoeche, H. Ita, D. A. Kosower, N. A. Lo Presti, and D. Maitre (2013), arXiv:1312.0592.

[73] Tech. Rep. ATL-PHYS-PUB-2013-009, CERN, Geneva (2013).

[74] G. Cowan, K. Cranmer, E. Gross, and O. Vitells, Eur.Phys.J. **C71**, 1554 (2011), arXiv:1007.1727.

[75] D. O'Connell, M. J. Ramsey-Musolf, and M. B. Wise, Phys.Rev. **D75**, 037701 (2007), hep-ph/0611014, and references therein.

[76] in preparation (2014).